

# A Study of Light-Sensitive Ideality Factor and Voltage-Dependent Carrier Collection of CdTe Solar Cells in Forward Bias

Zhitao Wang, Zimeng Cheng, Alan E. Delahoy, and Ken K. Chin

**Abstract**—Two features that distinguish CdS/CdTe solar cells from traditional c-silicon cells have been widely confirmed by experiment: 1) The ideality factor of the diode current is sensitive to photon flux input, and 2) the photocurrent is voltage dependent. Here, numerical simulation of one-sided p-type CdTe junctions has been performed in order to interpret the experimental characteristics under forward bias. In these calculations, we assumed a distribution of trapping states within the CdTe bandgap. Detailed discussions have been divided into two parts: light-dependent forward current and voltage-dependent carrier collection. The former has demonstrated that recombination loss increases with increased optical generation. As a result, the diode current, in a certain forward bias region, depends on illumination. With this mechanism, the ideality factor of simulated  $J$ - $V$  curves shows a variation consistent with experimental curves. Carrier collection loss under voltage bias is the combined result of carrier diffusion, drift, and recombination during transport. Simulations that are based on our assumption have demonstrated that collection loss increases at higher forward bias and depends on wavelength, carrier mobility, and carrier lifetime.

**Index Terms**—CdS/CdTe solar cells, photovoltaics, thin films.

## I. INTRODUCTION

IN the operation of solar cells, there are essentially two independent inputs that adjust the output current: applied voltage across the device and incident photon flux, both of which are implemented into the classical equation

$$J(\Phi, V) = J_0 \left[ \exp\left(\frac{qV}{AkT}\right) - 1 \right] - J_{\text{photo}}(\Phi) \quad (1)$$

where  $A$  denotes the ideality factor and  $\Phi$  the photon flux; the output current equals the diode current minus the photocurrent.

For high quality crystalline solar cells, the model describes the current-voltage curves very well: The diode current only depends on the applied voltage, and the photocurrent linearly responds to photon flux. Such a model is valid when the device (e.g., a crystalline-Si solar cell) has three major characteristics:

1) a high concentration of shallow dopants, which lead to a much smaller depletion width compared with the neutral region; 2) a very low density of traps; and 3) high carrier mobility. These conditions result in negligible carrier loss in the space charge region (SCR) and a long diffusion length in the neutral region. Therefore, the diode current is dominated by the diffusion current, and photocurrent is independent of voltage.

However, the classical equation fails to describe the actual  $I$ - $V$  curves of polycrystalline thin film solar cells (e.g.,  $n^+$ -CdS/p-CdTe cells) in two of their aspects: 1) In a certain low forward bias region, the diode current responds to photon flux, and its ideality factor under illumination is greater than 2; and 2) their photocurrent collection depends on the applied voltage, and therefore, their current-voltage curves under different light intensities fail to follow the linear superposition implied by (1).

In order to understand these unique features, one should distinguish the essential properties of  $n^+$ -CdS/p-CdTe solar cells from crystalline cells. First, CdTe is so weakly doped that the depletion width on the CdTe side can reach several micrometers. This may result in a different collection loss mechanism, which is dominated by carrier recombination in the widespread depletion region. Second, there may exist several types of trapping states within the bandgap of the CdTe, most of which also serve as nonshallow dopants ( $>0.01$  eV). There is much literature that reports the major defect states in CdTe, e.g., as a result of calculation [1], and from experiment [2]. Finally, the mobility of polycrystalline CdTe could be much lower than that of the crystalline material [3].

In this paper, it is assumed that these experimental deviations from the crystalline solar cells may be attributed to a generation-recombination (G-R) coupling mechanism that occurs via multiple trap states within the CdTe bandgap. As systematically discussed in [4], both dopants and traps should be treated on an equal footing, and may play the role as dopant and trap simultaneously. For example, a shallow-level acceptor state is efficient in donating holes but less efficient in electron-hole recombination while a deeper state possesses interchanged efficiencies for these processes. In thin-film CdTe solar cells, it is possible that there are no efficient shallow dopants but rather that there are multiple deeper acceptor-type states within the bandgap that provide a similar doping level. In other words, although the hole concentration is in the order of  $10^{14}$  /cm<sup>3</sup>, the concentration of acceptor states might be even higher, and their distribution might occur over a wide range within the bandgap of the CdTe. Therefore, these states also play critical roles in the Shockley-Read-Hall (SRH) recombination. In this paper, we explore the

Manuscript received December 2, 2012; revised January 23, 2013; accepted February 7, 2013. Date of current version March 18, 2013. This work was supported by the Apollo Solar Energy Research Center, Department of Physics, New Jersey Institute of Technology.

The authors are with New Jersey Institute of Technology, Newark, NJ 07102 USA (e-mail: zw56@njit.edu; zc6@njit.edu; delahoy@njit.edu; chin@njit.edu).

Color versions of one or more of the figures in this paper are available online at <http://ieeexplore.ieee.org>.

Digital Object Identifier 10.1109/JPHOTOV.2013.2247095

TABLE I  
BASELINE PARAMETERS IN THE CdTe LAYER

Symbol	Quantity	Value (Unit)
$d$	CdTe thickness	5 $\mu\text{m}$
$\epsilon/\epsilon_0$	dielectric constant	9.4
$\mu_n, \mu_p$	electron and hole mobility	100 $\text{cm}^2/\text{V/s}$ , 20 $\text{cm}^2/\text{V/s}$
$E_g$	band gap of CdTe	1.51 eV
$N_c$	effective density of states in conduction band	$9 \times 10^{18}/\text{cm}^3$
$N_v$	effective density of states in valance band	$1.8 \times 10^{19}/\text{cm}^3$
$\Delta\chi_c$	energy band offset between CdS and CdTe	0.1 eV
$\Delta E_{Fn}$	electron Fermi level of CdS below conduction band	0.08 eV
$N_A$	total acceptor states density	$10^{15}/\text{cm}^3$
$\Delta E$	distribution of acceptor states	0.15 eV to 0.85 eV
$\sigma_n, \sigma_p$	electron and hole capture cross-section	$10^{-13} \text{cm}^2$ , $10^{-13} \text{cm}^2$
$v_n, v_p$	thermal velocity of electrons and holes	$10^7 \text{cm/s}$ , $10^7 \text{cm/s}$
$S_n, S_p$	back surface recombination velocity of electrons, and holes	$10^6 \text{cm/s}$ , $10^4 \text{cm/s}$

Donor-type defects/states would also play dual roles in doping compensation and carrier recombination, both of which deteriorate the performance of the cells. To describe a clear mechanism of ‘‘G-R’’ coupling, we did not consider their potential effects in our simulation.

consequences of assuming that there are multiple acceptor-type states that are uniformly distributed in a wide range of the CdTe bandgap. To do this, we solve the basic semiconductor equations for the one-sided CdTe junction under illumination.

## II. FOUNDATION OF NUMERICAL SIMULATION

To solve the problem numerically, one needs three essential equations: Poisson’s equation, the electron and hole continuity equations, in which the electric potential  $\psi$ , electron current  $J_n$ , and hole current  $J_p$  are three independent variables from the following equations:

$$\frac{d^2\psi}{dx^2} = \frac{q}{\epsilon} \left[ p - n + \sum_L N_{AL} \frac{1}{1 + \frac{1}{g_A} \exp\left(\frac{E_{AL} - E_{Fp}}{kT}\right)} \right] \quad (2)$$

$$\frac{dJ_n}{dx} = -\frac{dJ_p}{dx} \quad (3a)$$

$$= \frac{q}{\epsilon} \left[ G - \sum_L \alpha_L N_{AL} \frac{np - n_i^2}{\beta_L (n + n_L^*) + \frac{1}{\beta_L} (p + p_L^*)} \right] \quad (3b)$$

where the subscript  $L$  represents different levels of dopant/trap in the bandgap;  $p, n, n_i, g_A, E_{Fp}, k, T$ , and  $G$  are the hole density, electron density, intrinsic carrier density, acceptor degeneracy, hole Fermi level in CdTe, Boltzmann constant, temperature, and the net optical generation rate, respectively. In these simulations,  $T$  was set at 300 K; the  $G$  was calculated (see [5]) from the incident photon flux that are based on the stated percentage of the standard AM1.5 Global solar spectrum. In tetrahedral cubic semiconductors,  $g_A = 4$  was used; other parameters are listed in Table I;  $n^*, p^*, \alpha$ , and  $\beta$  at certain energy level  $L$  are noted

as follows:

$$n^* = n_i \exp\left(\frac{E_i - E_A}{kT}\right) \quad (4a)$$

$$p^* = n_i \exp\left(\frac{E_A - E_i}{kT}\right) \quad (4b)$$

$$\alpha = \sqrt{\sigma_n \sigma_p v_n v_p} \quad (4c)$$

$$\beta = \sqrt{\sigma_n v_n / \sigma_p v_p}. \quad (4d)$$

Using the finite difference approximation, differentials become the ratio of variable difference to the interval step. By slicing the layer into  $N$  slabs, one needs to solve  $3N$  unknowns in  $3N - 6$  equations that are based on (2) to (3), which are combined with a total of six boundary conditions on both ends of the CdTe layer. The calculation approach is based on the Newton–Raphson method, similar to AMPS 1-D [6]. In our case, boundary conditions are appropriately fixed at the CdS/CdTe interface and at the end of the CdTe bulk. Compared with AMPS, our interest is only focused on the mechanism of SRH recombination within the CdTe bulk region. Table I shows the baseline parameters originally implemented into the simulation. The capture cross sections of electrons and holes are all assumed to be the same, with  $\sigma_n = \sigma_p = 10^{-13} \text{cm}^2$ , equivalent to  $\beta = 1$ , and  $\alpha = 10^{-6} \text{cm}^3/\text{s}$ . We believe that while some quantitative differences would result from assuming nonequal capture cross sections, the broad conclusions of our analysis would remain intact.

## III. EXPERIMENTAL DETAILS

### A. Sample Preparation

CdTe solar cells with about 10% efficiency were made with the structure: glass/TCO/ $n^+$ -CdS/ $p$ -CdTe/graphite/metal back contact (copper). Glass substrates that were coated with  $\text{SnO}_2:\text{F}$  plus HRT layer were used. CdS with a thickness of about 80 nm was deposited by chemical bath deposition (CBD) at 88  $^\circ\text{C}$  using cadmium chloride, thiourea, ammonium acetate, and ammonia, and was then annealed at 400  $^\circ\text{C}$ . The CdTe layer (6–10  $\mu\text{m}$ ) was deposited by close-spaced sublimation (CSS) at  $T_s = 600$   $^\circ\text{C}$  using graphite susceptors under 10–15 torr  $\text{He}/\text{O}_2$  [7]. A  $\text{CdCl}_2$ /methanol treatment was performed at 80  $^\circ\text{C}$ , which was followed by annealing in  $\text{He}/\text{O}_2$  at 380  $^\circ\text{C}$  and at 300 torr. Such treatment improves interfacial mixing of CdS and CdTe [8], and the presence of S within the CdTe may serve to passivate certain defect states. Before back contact deposition, the CdTe was etched by nitric-phosphoric (NP) acid to remove the surface oxide and then a thin layer of Cu was evaporated. Graphite paste that contained  $\text{ZnTe}:\text{Cu}$  was applied, which was followed by annealing in He at 160  $^\circ\text{C}$  and then a metallic electrode. This type of processing can be found in Rose’s paper [9].

### B. Current–Voltage Measurement

A vacuum-tight dewar (tubular stainless-steel chamber with optical side-windows) was used to measure the current–voltage characteristic of our samples at either room temperature or below. A white light LED array was used instead of a Xenon lamp

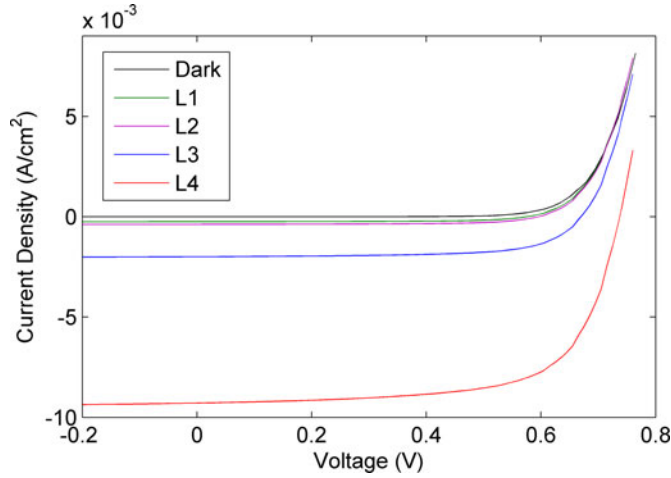


Fig. 1. Current–voltage curves under different light intensities.

TABLE II

*I*–*V* PERFORMANCE OF Cds/CdTe SOLAR CELLS UNDER VARIOUS INTENSITIES

Intensity	V <sub>oc</sub> (V)	J <sub>sc</sub> (mA/cm <sup>2</sup> )	FF (%)
L1	0.57	0.248	65.2
L2	0.596	0.379	65.8
L3	0.67	1.992	67.7
L4	0.73	9.284	67.8

to provide a steady light intensity for characterization. In this paper, the *I*–*V* measurement was carried out at room temperature from  $-0.2$  to  $0.76$  V applied bias to allow the current to reverse sign at the open-circuit voltage  $V_{oc}$ . A set of neutral density filters was used to reduce the light intensity when needed.

### C. Result

Fig. 1 shows the *I*–*V* curves of our sample in the dark and at four increasing intensities, L1, L2, L3, and L4. The performance of the cell with area  $0.25$  cm<sup>2</sup> at room temperature is listed in Table II. Any back barrier effect can be neglected in this voltage range since there is no roll-over effect around  $V_{oc}$ . However, a crossover between the dark and light *I*–*V* curve L1 does occur around  $0.68$  V. Such nonlinear superposition is likely due to a carrier collection loss as will be discussed in a later section. A focus on light-dependent ideality factor that is determined from experiment reveals interesting behavior which cannot be described by the classical model.

By compensation of photocurrents, all *I*–*V* curves were shifted to the origin and their ideality factors were determined from the slopes of the current in natural logarithmic scale, as shown in Fig. 2. Four major features are pointed out: 1) Diode currents in low forward bias ( $0$  to  $0.6$  V, region I) are activated by illumination in terms of ideality factors greater than 2; 2) as photon flux is increased, ideality factors tend to increase slightly, and from  $A \approx 5$  at low light level L1 to  $A \approx 7$  at higher light level L4; 3) as voltage is increased, ideality factors of all illuminated *I*–*V* curves tend to the same value as that of the dark diode current and region II applies; 4) the transition between these two regions shifts to lower voltage as light intensity is reduced.

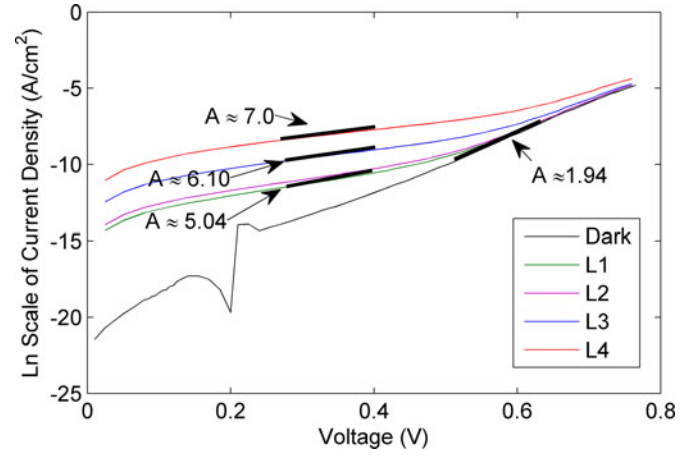


Fig. 2. Diode current density in natural logarithmic scale under different levels of light injection.

Since fairly standard processing steps were used in fabrication the cells, the aforementioned findings would appear to be generally applicable to CdTe cells. Similar characteristics of these curves can also be found in [10]. One might argue that the rise of the curves in a low-voltage region is due to light-dependent shunt resistance [11], [12]. Such a mechanism is characterized by a large increase in the fill factor at low light levels. In contrast, Table II shows a small decrease in the fill factor at reduced light levels. Therefore, it is suggested that such a shunting effect should be excluded. In any case, the observed light-dependent behavior exhibits characteristics consistent with our modeling result, as discussed in the following.

## IV. LIGHT-DEPENDENT SHOCKLEY–READ–HALL RECOMBINATION CURRENT

### A. Mechanism of Generation–Recombination Coupling

In the case of study, we only consider the steady-state condition. The SRH equation [13] can be rewritten in the concise expression:

$$U_{SRH}(x) = \frac{\alpha N_t n_i^2 \left\{ \exp \left[ \frac{q(E_{Fn}(x) - E_{Fp}(x))}{kT} \right] - 1 \right\}}{\beta (n + n^*) + \frac{1}{\beta} (p + p^*)}. \quad (5)$$

Therefore, then the SRH recombination current  $J_{SRH}$  can be calculated by the integral of the recombination rate  $U_{SRH}(x)$  throughout the CdTe region. In (5),  $U_{SRH}$  strongly depends on quasi-Fermi levels  $E_{Fn}$  and  $E_{Fp}$ . Note that there are significant differences between the dark and light conditions. For example, without photon flux,  $E_{Fn}$  and  $E_{Fp}$  at zero bias (see Fig. 3) overlap at  $0.3$  eV from  $0$  to  $5$   $\mu$ m. Therefore, recombination at zero bias does not contribute, according to (5).

However, this is no longer true in the case of illumination. When a majority of photons are absorbed in the SCR of CdTe, these photoexcited electron–hole pairs create a new steady-state condition for the electron and hole quasi-Fermi levels. Still with  $0$  V bias (see Fig. 3), the minority carrier density increases, which is equivalent to the rise of  $E_{Fn}$  (red) from the depletion region to the neutral region. Similarly, the majority carrier

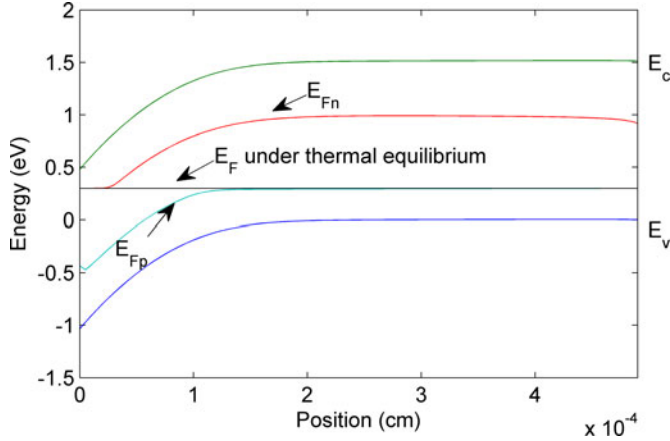


Fig. 3. Schematic band diagram of CdTe under dark and one sun at zero bias. Numerical calculation applied finite difference method at 50 nm interval from the interface between CdS and CdTe (position 0  $\mu\text{m}$ ) to the end of bulk (5  $\mu\text{m}$ ). Energy band bending within the CdS and effect of back contact is not considered.

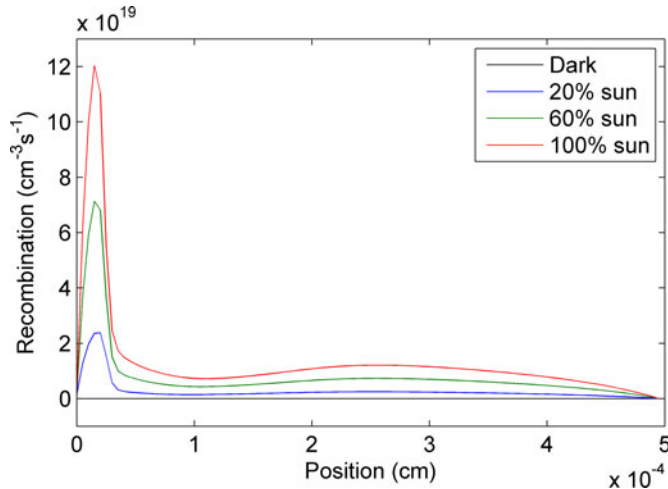


Fig. 4. Spatial distribution of SRH recombination rate under various illumination intensities at  $V = 0$  V.

density increases within the SCR region, which corresponds to lowering of  $E_{Fp}$  (light blue); however, the density of those photoexcited holes in the depletion region is minor compared with the bulk hole density ( $p = 10^{14} \text{ cm}^{-3}$ ). Because of the high concentration of defects/acceptor state within the bandgap, SRH recombination is present (in the light) even at zero bias. When the optical generation rate is increased, more photogenerated carriers will participate in recombination via these traps. In other words, recombination couples with optical generation.

The simulation in Fig. 4 plots the distribution of recombination from the front interface (on the left) to the end of the bulk region (on the right). Under dark condition, SRH recombination at zero bias equals zero throughout the CdTe region, which agrees with the aforementioned discussion. However, with increase in photon flux, the recombination rate increases in both the depletion region and the neutral region. A large portion of the recombination occurs within 300 nm, which starts from the interface. Although the contribution of the bulk region seems

minor, the width of the recombination peak extends through a few micrometers in the neutral region. When there is a high concentration of defects that are located within the neutral region, the integral of recombination cannot be neglected in the neutral region. In the case, we have modeled, even for low defect concentration ( $N_t = 10^{15} \text{ cm}^{-3}$ ), the SRH current density under illumination can be a few milliamps per unit area (e.g.,  $J_{\text{SRH}} \approx 2 \text{ mA/cm}^2$ , at 0 V), and such an increasing contribution at increased voltage results from the SCR (e.g., over 80% of recombination occurs within the SCR at  $V_{\text{mp}} \approx 0.68$  V, the voltage at maximum power output).

Analysis of the G–R coupling effect can be split into depletion and neutral regions as follows:

$$1) n_D \gg \Delta p_L \gg p_D.$$

Such a condition applies to the depletion region. In this region (between 0 and 300 nm), the electron density (in the order of  $10^{15} \text{ cm}^{-3}$ ) dominates over the hole density due to high electron carrier injection from the CdS layer. Assuming  $\beta = 1$ , the SRH equation can be approximated as follows:

$$U_{\text{SRH}} \approx \frac{\alpha N_t (n_D \Delta p_L - n_i^2)}{n_D + n^* + p^*}. \quad (6)$$

In (6), only the light-induced hole concentration  $\Delta p_L$  depends on photon flux. Aside from other parameters independent of optical generation,  $n^*$  and  $p^*$  are also constant, as they are only related to trapping energy levels. Thus, optical generation rate modulates  $\Delta p_L$ , and as a result,  $U_{\text{SRH}}$  responds. Since the electron density reduces dramatically within less than half a micrometer from the interface, the recombination rate likewise decreases dramatically. A transition from the first condition to the second occurs as follows:

$$2) n_D \ll \Delta n_L \ll p_D.$$

This condition is valid in the neutral region ( $\Delta n_L \sim 10^9 \text{ cm}^{-3}$ ,  $p_D \sim 10^{14} \text{ cm}^{-3}$ ). The SRH equation can be approximated as follows:

$$U_{\text{SRH}} \approx \frac{\alpha N_t (\Delta n_L p_D - n_i^2)}{n^* + p_D + p^*}. \quad (7)$$

Under low optical injection, the concentration of light-induced holes  $\Delta p_L$  is much lower than  $p_D$  in the dark, which leads to the dominating term  $p_D$  in the denominator. However, since  $\Delta n_L$  is greater than  $n_D$ , the G–R coupling is due to photoexcited electrons in this region.

### B. Illuminated Shockley–Read–Hall Current in Forward Bias

After solving for the band bending unknowns, namely, the electric potential  $\psi$ , the electron quasi-Fermi level  $E_{Fn}$ , and the hole quasi-Fermi level  $E_{Fp}$  as a function of position that is based on (2) to (3b), the SRH current can be calculated as a function of voltage. The simulation was carried out from 0 to 0.8 V at 0.02 V intervals. According to the continuity equation, the total output current equals

$$\begin{aligned} J &= q \cdot \int U_{\text{SRH}}(x, V, \Phi) dx - q \cdot \iint G(x, \lambda, \Phi_\lambda) d\lambda dx \\ &= J_{\text{SRH}}(V, \Phi) - J_{\text{photo}}(\Phi). \end{aligned} \quad (8)$$

TABLE III  
SIMULATED PERFORMANCE OF CdS/CdTe SOLAR CELLS UNDER  
VARIOUS INTENSITIES

Intensity	Voc (V)	Jsc (mA/cm <sup>2</sup> )	FF (%)
1% sun	0.68	0.23	66.4
20% sun	0.72	4.70	69.6
60% sun	0.77	14.1	70.2
100% sun	0.78	23.4	67.7

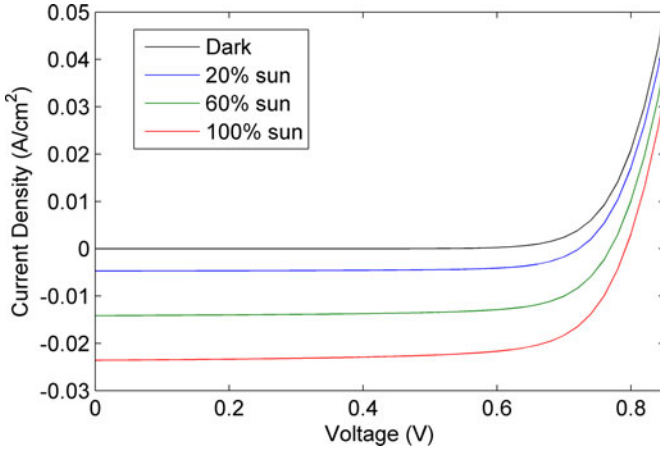


Fig. 5. Simulation of output current versus voltage under different photon fluxes.

Note that the first term, the SRH recombination current, becomes a function of the applied voltage and photon flux. Compared with (1), the diode current also depends on light injection, which is due to G–R coupling. The second term, which is the ideal photocurrent  $J_{\text{photo}}$ , is only a function of photon flux  $\Phi$ . Table III is a list of calculated results using the initial parameters that are presented in Table I.

Fig. 5 shows output current  $J$  under different photon fluxes. By increasing photon flux, light-induced recombination currents become more apparent in low forward bias (0–0.6 V). Then, such a G–R coupling effect begins to saturate at higher voltages. Fig. 6 replots the  $J$ – $V$  curves on a natural logarithmic scale. Extrapolated ideality factors indicate very similar characteristics as the experimental data: 1) From dark to 1% one sun illumination, the ideality factor of SRH currents in Region I (0–0.6 V) jumps from 1.7 to 6.2. Therefore, this region tends to be light activated; 2) ideality factors increase slightly from  $A \approx 7.2$  at 20% of one sun level to  $A \approx 7.7$  at full sun level; 3) in Region II, the slopes of all curves converge to that of the dark SRH current; and 4) the transition from Region I to Region II shifts to higher voltage as light injection is enhanced.

The discussion of these characteristics can be separated into Region I and Region II.

*Region I* ( $n_D \gg \Delta p_L \gg p_D$ ): We can approximate the SRH recombination to that within the SCR region since it provides the major contribution. Then, (6) applies in Region I between 0 and 0.6 V. Since the increased applied voltage reduces the electric field within the depletion region, carriers are more likely to accumulate, which lead to the increase in electron and hole

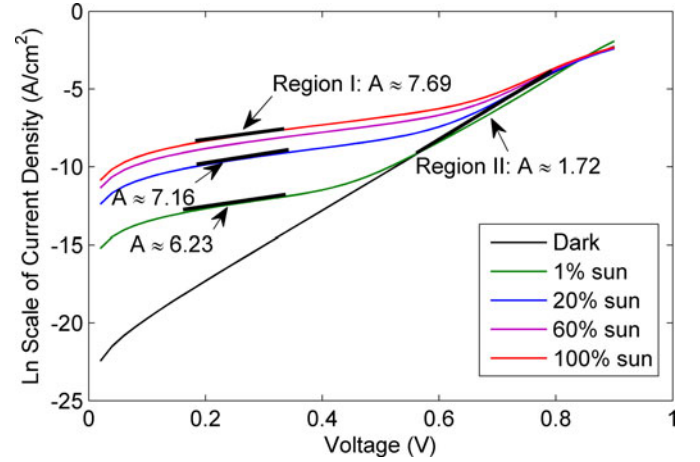


Fig. 6. Logarithmic plot of the SRH current. Each curve in Fig. 5 is shifted up to its output current at zero bias. Ideality factors under illumination change with photon flux and voltage bias.

densities. Note that  $n$  is composed of electrons in dark  $n_D$  and light-induced electrons  $\Delta n_L$ , with the same notation for holes. However,  $\Delta n_L$  is orders of magnitude lower than  $n_D$  due to high electron injection from the CdS/CdTe interface, whereas  $\Delta p_L$  could be larger than  $p_D$  nearby the interface in Region I. Upon biasing to higher voltage, the SRH recombination becomes even more sensitive to light-induced  $\Delta p_L$  due to the larger factor of  $n_D$ . Further bias voltage beyond 0.6 V increases  $p_D$  in the SCR region. When  $\Delta p_L$  is of the same order of  $p_D$ , transition occurs and Region II begins to be activated. Therefore, the more  $\Delta p_L$  generated by stronger light intensity, the higher forward voltage is required to increase  $p_D$  to be same level as  $\Delta p_L$ .

*Region II* ( $n_D \gg p_D > \Delta p_L$ ): In this case,  $p_D$  grows larger than  $\Delta p_L$ ; however, the effect of  $\Delta p_L$  cannot be neglected. The SRH equation becomes

$$U_{\text{SRH}} \approx \frac{\alpha N_t [n_D (p_D + \Delta p_L) - n_i^2]}{n^* + n_D + p^*}. \quad (9)$$

Although both  $p_D$  and  $\Delta p_L$  contribute in this region, the growth rate of  $U_{\text{SRH}}$  is limited by  $p_D$ . Thus, the ideality factor tends to be the same as in the dark.

## V. VOLTAGE-DEPENDENT CARRIER COLLECTION

### A. Experimental Details

It has been reported that the illuminated  $J$ – $V$  curve fails to follow linear superposition, and that quantum efficiency also demonstrates strong dependence on voltage, in many thin-film solar cells [14], such as  $\alpha$ -Si [15], CuInSe<sub>2</sub> [16], and CdTe [17]. In the case of CdTe, the photogenerated carrier transport may lead to collection loss, and this phenomenon may account for the observations in other cell types. The voltage-dependent collection efficiency (CE,  $\eta_c$ ) has been previously introduced [18], [19] to quantify the photocurrent loss

$$\eta_c(V) = \frac{J_L(V, \Phi)}{J_{\text{photo}}(\Phi)} \quad (10)$$

where the collection efficiency is defined as the ratio of the photocurrent  $J_L(V, \Phi)$  at a given voltage to the ideal photocurrent  $J_{\text{photo}}(\Phi)$  under the total photon flux  $\Phi$ , which is integrated by all usefully absorbed incident photons:

$$J_{\text{photo}}(\Phi) = q \cdot \iint G(x, \lambda, \Phi_\lambda) d\lambda dx. \quad (11)$$

As proposed by Hegedus, the collection efficiency can be experimentally deduced by taking the difference between two illuminated  $J$ - $V$  curves:

$$\eta_c(V) = -\frac{J_1(V, \Phi_1) - J_2(V, \Phi_2)}{J_{\text{photo}}(\Phi_1) - J_{\text{photo}}(\Phi_2)} \quad (12)$$

where  $J_1$  and  $J_2$  are the output currents that are measured under two different photon fluxes  $\Phi_1$  and  $\Phi_2$ , respectively, and the ideal photocurrent  $J_{\text{photo}}(\Phi_1)$  and  $J_{\text{photo}}(\Phi_2)$  can be approximated by the short-circuit currents, or determined under reverse bias.

The underlying condition for the derivation from (10) to (12) is based on the assumption that CE under  $\Phi_1$  is equivalent to CE under  $\Phi_2$ . If so, the collection model can be rewritten as

$$J(\Phi, V) = J_F(V) - J_{\text{photo}}(\Phi) \eta_c(V) \quad (13)$$

In (13), the diode current is independent of photon flux  $\Phi$ , and the photocurrent is the multiplication of the ideal photocurrent and a collection function. However, one has to consider other external effects as pointed out by Gloeckler and Sites [19]; for instance, 1) under illumination, forward current may differ from the dark current due to photoconductivity effects, given some charges may be trapped in deep states and physical parameters deviate from dark condition; 2) the existence of series resistance may generate another experimental artifact, which apparently diminishes internal photo collection; 3) a high back contact barrier may also lead to cross over at lower voltage, and therefore, there is a considerable reduction in CE near the open-circuit voltage. In other words, the actual CE should exclude these effects; otherwise, collection loss due to carriers transport may be exaggerated.

The experimentally deduced collection efficiency has been calculated from the previous  $I$ - $V$  data under various photon fluxes as shown in Fig. 7. Any photoconductivity effect has been avoided by subtracting two illuminated currents under different light intensities. Fig. 7 shows that CE that is calculated from different combinations of light  $I$ - $V$  curves all exhibit the same tendency of collection loss with increased voltage bias. The collection efficiencies that are calculated from L2-L4 and L1-L4 overlap well with each other and reveal a reduction of more than 40%: from 0 to 0.8 V. The CE that is calculated from L2-L3 shows slight increase in collection loss around 0.6 V relative to the other curves, but we do not consider this significant.

### B. General Principle of Collection Efficiency Characterization

We now describe the physical processes that underlie the collection efficiency and our recommendation for a preferred method of measurement.

1) Under a steady background light with photon flux  $\Phi_1$ , the total output current  $J_1$  that is based on the continuity equation

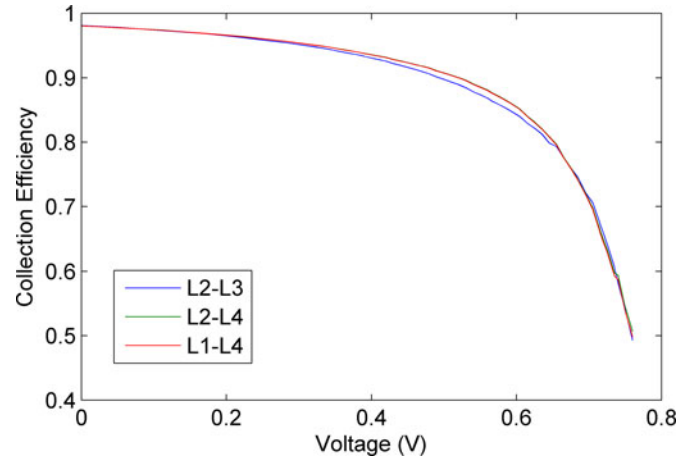


Fig. 7. Experimental collection efficiency calculated by (12), using different combination sets of illuminated currents.

is given by

$$J_1(V, \Phi_1) = J_F(V, \Phi_1) - J_{\text{photo}}(\Phi_1). \quad (14)$$

The first term  $J_F$  represents the forward current, which combines the carrier diffusion, drift, and recombination mechanisms. For example, excess photo-generated minority carriers outside the SCR will first diffuse through the neutral region, then drift in the electric field within the SCR, and, finally, be collected in the CdS layer; those prevented from completing the process have participated in recombination via multiple levels of trapping states, which include the G-R coupling and light-dependent SRH current. Therefore, the forward current is the net effect of carrier diffusion, drift, and recombination. The second term  $J_{\text{photo}}(\Phi_1)$  is the ideal photocurrent in (11) under photon flux  $\Phi_1$ , which is the spatial optical generation rate integrated over the thickness of the device.

2) When a much weaker light is superposed onto background light (e.g., for QE measurement, the probe beam is monochromatic light chopped at one certain frequency), the total current  $J_2$  becomes

$$J_2(V, \Phi_1 + d\Phi) = J_F(V, \Phi_1 + d\Phi) - J_{\text{photo}}(\Phi_1 + d\Phi). \quad (15)$$

By decomposing the forward current into two terms, we may write

$$J_F(V, \Phi_1 + d\Phi) = J_F(V, \Phi_1) + \Delta J_F(V, d\Phi) \quad (16)$$

where  $\Delta J_F$  represents the slight change in forward current that is induced by the probe beam with photon flux  $d\Phi$ .

This differential approach to collection efficiency was introduced in [5] and, in distinction to Hegedus' definition, has the advantage that the cell operating point is definitively fixed by the bias light. Inserting (14)–(16) into (12), we can derive an expression for the collection efficiency

$$\eta_c(V, d\Phi) = 1 - \frac{\Delta J_F(V, d\Phi)}{J_{\text{photo}}(\Phi_1 + d\Phi) - J_{\text{photo}}(\Phi_1)}. \quad (17)$$

In summary, the principle of measuring collection efficiency is based on subtracting two output currents at different

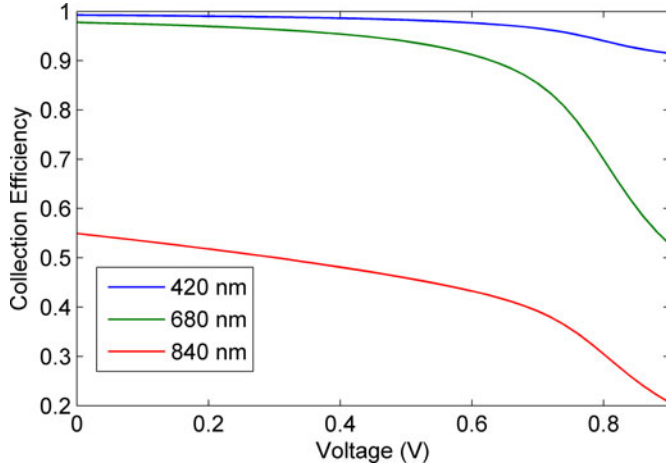


Fig. 8. Simulated collection efficiency under different weak monochromatic light superposed on one-sun background light.

intensities. Equations (14) through (17) assert that the collection loss that we measured actually derives from the change in diode current  $\Delta J_F$  that is induced by the superposed probe beam. Note that although (17) is an implicit function,  $\Delta J_F$  represents the combined effect of carrier diffusion, drift, and recombination.

### C. Simulation and Discussion

Collection loss occurs in two regions: the SCR and the neutral region. In the SCR, the strength of electric field and the depletion width both decrease with increased forward voltage, which increases the overall importance of carrier diffusion. The reduced electric field within the SCR leads to accumulated carriers and increased recombination via trapping centers. The CE becomes smaller for minority carriers that are generated in the neutral region than in the SCR due to the much shorter diffusion length than drift length in CdTe. In general, a new equilibrium condition is reached until diffusion, drift, and recombination further balance again.

Numerical simulation of CE as a function of the applied voltage has been studied in three aspects: 1) spectral response of CE; 2) the impact of mobility  $\mu_n$  and  $\mu_p$  on CE; and 3) the impact of minority carrier lifetime on CE. All initial parameters remain the same as in Table I, except the one that is to be studied.

1) *Collection Efficiency Under Monochromatic Light*: Investigation of collection loss within the CdTe layer has been conducted at three representative wavelengths: 420, 680, and 840 nm. The absorption coefficients of CdTe at these wavelengths are  $1.9 \times 10^5 \text{ cm}^{-1}$ ,  $3.7 \times 10^4 \text{ cm}^{-1}$ , and  $7 \times 10^2 \text{ cm}^{-1}$ , respectively [20]. Calculation of CE using (12) compares the  $J$ - $V$  curves under one-sun full spectrum illumination with another under additional weak monochromatic light superposed onto the original illumination.

Fig. 8 shows that the CE for strongly absorbed blue light slightly decreases at high forward bias, whereas at longer wavelengths, CE declines more dramatically. As wavelength approaches the band edge of CdTe, the collection loss becomes significant even at 0 V (red curve). The results indicate that the SCR collection is the dominant process for strongly absorbed

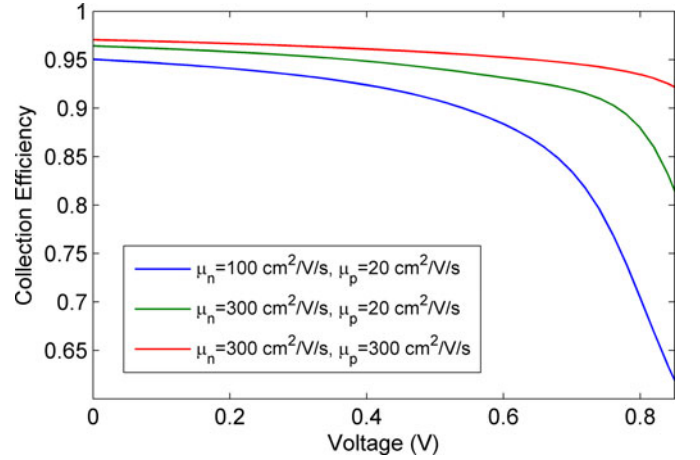


Fig. 9. Simulated collection efficiency on the CdTe layer with various mobility parameters.

light, since more than 90% of the electron-hole pairs are generated within the SCR. However, at longer wavelengths, the combination of SCR and neutral region transport occurs. The CE at 680 nm demonstrates that a high CE exists at small bias voltages due to efficient carrier drift within SCR, whereas diffusion becomes more significant at higher voltages due to reduced depletion width and electric field [5]. For weakly absorbed light near the band edge, most carriers will be generated outside the SCR. Therefore, carrier diffusion and recombination account for the large collection loss at zero bias.

2) *Influence of Mobility on Collection Efficiency*: Mobility affects both diffusion length in the neutral region and drift length in the SCR. Fig. 9 demonstrates that when diffusion and drift lengths are reduced by carrier mobility, collection efficiency decreases significantly at high forward bias. Each curve was calculated by the difference of two  $J$ - $V$  curves under 20% and 100% of one-sun white light that is based on (12). The variation of CE curves indicates that as diffusion and drift length fall due to reduced mobility, more carriers will participate in recombination before they reach to the electrodes. With increased forward voltage, more carriers accumulate and recombine within the SCR due to reduced electric field. Therefore, the loss in CE in a high forward bias region is dominated by increased recombination loss within the SCR.

3) *Influence of Minority Carrier Lifetime on Collection Efficiency*: The collection loss that is attributed to SRH recombination during the process of carrier transport can also be characterized by minority carrier lifetime. In the p-type CdTe bulk region, the lifetime is limited by the SRH recombination, which can be approximated by

$$\tau = \frac{\Delta n}{U_{\text{SRH}}} \quad (18)$$

where  $\Delta n$  is the light-induced electron density.

The recombination rate  $U_{\text{SRH}}$  can be adjusted according to (5) by simply keeping  $\sigma_n = \sigma_p$  ( $\beta = 1$ ) but varying their sizes in terms of changing  $\alpha$ . The spatial distribution of carrier lifetime at 0 V that was calculated from (18) is plotted in Fig. 10. The steep fall of  $\tau$  from 0 to 300 nm is due to the dramatic decrease

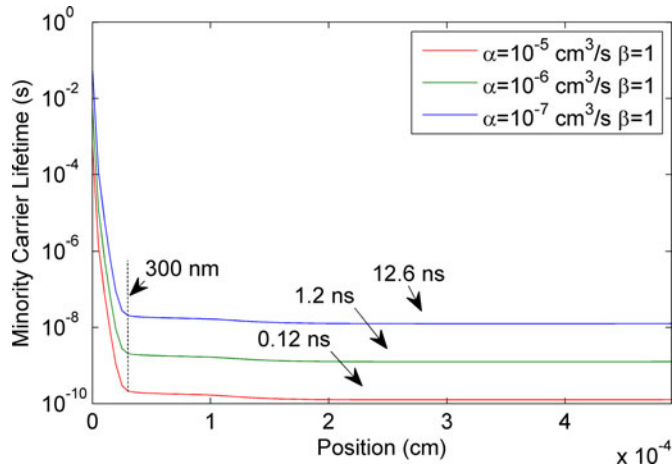


Fig. 10. Spatial distribution of SRH lifetime under one-sun illumination at 0 V using different  $\alpha$  data. (From left to right: CdS/CdTe interface at 0  $\mu\text{m}$  to the end of CdTe bulk at 5  $\mu\text{m}$ .)

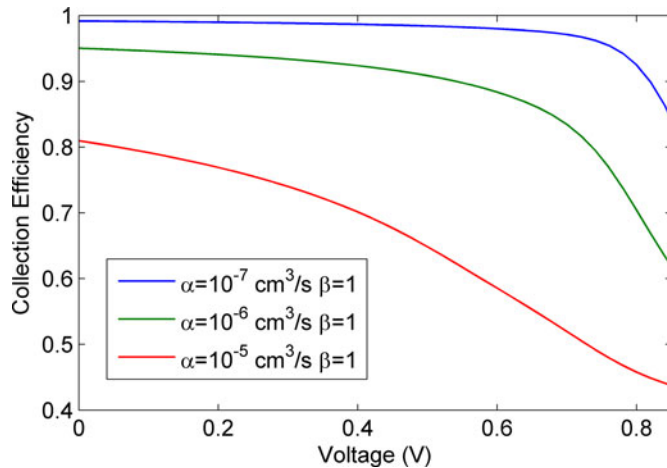


Fig. 11. Simulated collection efficiency of CdTe with different lifetime data. (For values, see Fig. 10.)

in  $\Delta n$ , which then starts to stabilize. Note that  $\tau$  after 300 nm is determined by  $U_{\text{SRH}}$  in (18). As the factor  $\alpha$  in  $U_{\text{SRH}}$  is reduced by one order of magnitude, minority carrier lifetime  $\tau$  is also improved by one order correspondingly.

The averaged lifetime from the interface to the boundary between the SCR and quasi-neutral regions is critical to collection loss since more than 95% of photons will be absorbed within 1350 nm (from the left) under AM 1.5 solar spectrum irradiation, where such boundary is generally located.

Fig. 11 plots the CE as a function of voltage, which was calculated via the subtraction of  $J$ - $V$  curves under 20% and 100% one-sun illumination. A shorter carrier lifetime reflects higher SRH recombination rate within the SCR, and therefore, there is a significant drop in the CE with increased geometric factor  $\alpha$  and bias voltage. Moreover, it can be concluded that the collection loss due to SRH recombination can be reduced by improved lifetime, and the reduced collection loss will improve the fill factor of the solar cells.

## VI. CONCLUSION

In CdTe solar cells, it is possible that there is no effective (i.e., shallow) dopant but that multiple states within the bandgap play the role of nonshallow dopant and trap simultaneously. Therefore, the diode current in forward bias, both in the dark and in the light, can be approximated by SRH recombination current. Simulation of SRH current has demonstrated certain characteristics that include a light-dependent ideality factor. These predictions follow a similar trend to observations on our lab cell and to those in [9]. A detailed discussion with regard to the SRH current was presented to analyze those characteristics. It is concluded that as optical generation increases, more carriers are lost to recombination via these states. This G-R coupling mechanism has a significant impact on the SRH current in terms of an extraordinary illuminated ideality factor greatly exceeding 2, which cannot be reasonably explained by a classical model for crystalline devices.

It has also been discussed that collection loss in forward bias rests on three electronic mechanisms: carrier diffusion, carrier drift, and carrier recombination. Simulation of the collection efficiency demonstrated that internal collection losses within the CdTe layer become significant at higher forward bias and depend on the wavelength, mobility, and lifetime.

## ACKNOWLEDGMENT

The authors would like to thank G. Liu for CdS depositions in early stage of sample preparation.

## REFERENCES

- [1] S.-H. Wei and S. B. Zhang, "Chemical trends of defect formation and doping limit in II-VI semiconductors: The case of CdTe," *Phys. Rev. B*, vol. 66, pp. 155211-1–155211-10, 2002.
- [2] H. Elhadidy and J. Franc, "Deep level defects in CdTe materials studied by thermoelectric effect spectroscopy and photo-induced current transient spectroscopy," *Semicond. Sci. Technol.*, vol. 22, pp. 537–542, 2007.
- [3] M. Miyake, K. Murase, T. Hirato, and Y. Awakura, "Hall effect measurements on CdTe layers electrodeposited from acidic aqueous electrolyte," *J. Electroanal. Chem.*, vol. 562, pp. 247–253, 2004.
- [4] K. K. Chin, "Dual roles of doping and trapping of semiconductor defect levels and their ramification to thin film photovoltaics," *J. Appl. Phys.*, vol. 111, pp. 104509-1–104509-9, 2012.
- [5] A. E. Delahoy, Z. Cheng, and K. K. Chin, "Carrier collection in thin-film CdTe solar cells: Theory and experiment," in *Proc. 27th EU PVSEC*, 2012, pp. 2837–2842.
- [6] AMPS 1-D Manual, Center Nanotechnol. Edu. Utilization, Penn. State Univ., University Park, PA, USA, 2010.
- [7] T. C. Anthony, A. L. Fahrenbruch, and R. H. Bube, "Growth of CdTe films by close-spaced vapor transport," *J. Vac. Sci. Technol. A*, vol. 2, p. 1296, 1984.
- [8] B. E. McCandless and K. D. Dobson, "Processing options for CdTe thin film solar cells," *Sol. Energy*, vol. 77, pp. 839–856, 2004.
- [9] D. H. Rose, F. S. Hasoon, R. G. Dhere, D. S. Albin, R. M. Ribelin, X. S. Li, Y. Mahathongdy, T. A. Gessert, and P. Sheldon, "Fabrication procedures and process sensitivities for CdS/CdTe solar cells," *Prog. Photovolt. Res. Appl.*, vol. 7, pp. 331–340, 1999.
- [10] D. L. Liam, V. P. Singh, J. C. McClure, G. B. Lush, X. Mathew, and P. J. Sebastian, "Light and voltage dependence of the junction transport properties of CdTe/CdS photovoltaics," *Sol. Energy Mat. Sol. Cells*, vol. 70, pp. 335–344, 2001.
- [11] I. Riedel, J. Parisi, V. Dyakonov, L. Lutsen, D. Vanderzande, and J. C. Hummelen, "Effect of Temperature and illumination on the electrical characteristics of polymer-fullerene bulk-heterojunction solar cells," *Adv. Funct. Mater.*, vol. 14, no. 1, pp. 38–44, 2004.



- [12] S. Yoo, B. Domercq, and B. Kippelen, "Intensity-dependent equivalent circuit parameters of organic solar cells based on pentacene and C60," *J. Appl. Phys.*, vol. 97, pp. 103706-1–103706-9, 2005.
- [13] S. Sze, *Physics of Semiconductor Devices*, 2nd ed. New York, NY, USA: Wiley, 1981.
- [14] R. Crandall, "Modeling of thin film solar cells, uniform field approximation," *J. Appl. Phys.*, vol. 54, p. 7176, 1983.
- [15] S. Hegedus, "Current-voltage analysis of a-Si and a-SiGe solar cell including voltage-dependent photocurrent collection," *Prog. Photovolt.*, vol. 12, pp. 155–168, 2004.
- [16] M. Eron and A. Rothwarf, "Effects of a voltage-dependent light-generated current on solar cell measurements: CuInSe<sub>2</sub>/Cd(Zn)S," *Appl. Phys. Lett.*, vol. 44, pp. 131–133, 1984.
- [17] K. Mitchell and A. Fahrenbruch, "Evaluation of the CdS/CdTe heterojunction solar cells," *J. Appl. Phys.*, vol. 48, p. 4365, 1977.
- [18] S. Hegedus, "Voltage dependent photocurrent collection in CdTe/CdS solar cells," *Prog. Photovolt, Res. Appl.*, vol. 15, pp. 587–602, 2007.
- [19] M. Gloeckler and J. R. Sites, "Quantum efficiency of CdTe solar cells in forward bias," *Proc. 19th EU PVSEC*, pp. 1863–1866, 2004.
- [20] T. Myers, S. Edwards, and J. Schetzina, "Optical properties of polycrystalline CdTe films," *J. Appl. Phys.*, vol. 52, no. 6, pp. 4231–4237, 1981.

Authors' photographs and biographies not available at the time of publication.